Utilizing Rapid Hydrogen Peroxide Generation from 6-Hydroxycatechol to Design Moisture-Activated, Self-Disinfecting Coating

*Fatemeh Razaviamri[a], Sneha Singh[b], James Manuel[a], Zhongtian Zhang[a], Lynn M. Manchester[b], Caryn L. Heldt[b], Bruce P. Lee[a]**

[a]Department of Biomedical Engineering, Michigan Technological University, Houghton, Michigan 49931

[b]Department of Chemical Engineering, Michigan Technological University, Houghton, Michigan 49931

KEYWORDS: Reactive oxygen species, 6-Hydroxycatechol, Catechol, Antiviral, Antibacterial, Self-disinfecting coating

ABSTRACT: A coating that can be activated by moisture found in the respiratory droplets could be a convenient and effective way to control the spread of airborne pathogens and reduce fomite transmission. Here, the ability for a novel 6-hydroxycatechol-containing polymer to function as a self-disinfecting coating on the surface of polypropylene (PP) fabric was explored. Catechol is the main adhesive molecule found in mussel adhesive proteins. Molecular oxygen found in an aqueous solution can oxidize catechol and generate a known disinfectant, hydrogen peroxide (H_2O_2), as a

byproduct. However, given the limited amount of moisture found in respiratory droplets, there is a need to enhance the rate of catechol autoxidation to generate antipathogenic levels of H_2O_2. 6-Hydroxycatechol contains an electron donating hydroxyl group on the 6-position of the benzene ring, which makes catechol more susceptible to autoxidation. 6-Hydroxycatechol-coated PP generated over 3,000 μM of H_2O_2 within 1 h when hydrated with a small amount of aqueous solution (100 μL of PBS). The generated H_2O_2 was 3 orders of magnitude higher when compared to the amount generated by unmodified catechol. 6-Hydroxycatechol-containing coating demonstrated a more effective antimicrobial effect against both Gram-positive (*Staphylococcus aureus* and *Staphylococcus epidermidis*) and Gram-negative (*Pseudomonas aeruginosa* and *Escherichia coli*) bacteria when compared to unmodified catechol. Similarly, the self-disinfecting coating reduced the infectivity of both bovine viral diarrhea virus and human coronavirus 229E by as much as 2.5 log reduction value (a 99.7% reduction in viral load). Coatings containing unmodified catechol did not generate sufficient H_2O_2 to demonstrate significant virucidal effects. 6-Hydroxycatechol-containing coating can potentially function as a self-disinfecting coating that can be activated by the moisture present in respiratory droplets to generate H_2O_2 for disinfecting a broad range of pathogens.

1. Introduction

Airborne and contact transmission of infections through respiratory droplets have posed a significant global challenge during various respiratory infection outbreaks in history, such as coronavirus disease 2019 (COVID-19), Middle East respiratory syndrome (MERS), and severe acute respiratory syndrome (SARS), leading to a devastating number of deaths worldwide [1, 2]. Respiratory droplets are tiny particles of fluid (5 to 1,000 μm in diameter)[3, 4] that can carry infectious pathogens, including viruses and bacteria, and are expelled when an infected individual

coughs, sneezes, talks, or even breathes [5-7]. These droplets can travel through air, potentially reaching and infecting susceptible individuals [8, 9]. Additionally, they could come into contact with surfaces, potentially leading to surface contamination [10]. Therefore, antipathogenic methods are necessary to prevent the spread of infection through inhalation or indirect contact with contaminated surfaces. Using self-disinfecting face masks [11, 12] or surfaces [13] is a convenient and effective approach to control the spread of infections while reducing exposure to disinfectant products, which may cause health problems [14]. Currently available self-disinfecting methods [12, 15-25] rely on external factors such as heat [16] or light [17] or may not offer rapid disinfection, making them inconvenient or impractical for on-demand use. Hence, achieving rapid and effective antipathogenic performance is essential when designing self-disinfecting coatings.

Reactive oxygen species (ROS) are highly reactive molecules derived from the reduction of molecular oxygen (O_2) [26]. Hydrogen peroxide (H_2O_2) is a potent oxidizer [27] and has been demonstrated to function as a broad-spectrum biocide in various industrial and biomedical applications [28, 29]. H_2O_2 is also an attractive disinfectant as it degrades into water and oxygen [30]. However, the storage and transport of ROS pose significant challenges [30]. Diluted solutions of H_2O_2 are challenging to transport due to their bulkiness, while concentrated solutions pose risks during transportation because of their instability and explosive nature [30]. A practical solution to overcome these challenges is the use of polymers that could generate H_2O_2 on-demand. Specifically, we seek to design a novel, self-disinfecting coating that could be activated to generate ROS utilizing moisture found in the respiratory droplets.

Catechol is the main adhesive molecule found in mussel adhesive proteins, which enables these organisms to anchor to wet surfaces even in turbulent conditions [31-33]. Incorporation of catechol into a polymer system has been often utilized to design strong adhesives and coatings for a wide

range of applications [34-37]. During the process of catechol oxidation, ROS, such as H_2O_2, is generated as a byproduct [38, 39]. Our lab utilized this unique catechol oxidation chemistry to create biomaterials that can be activated to generate H_2O_2 through simple hydration [40-43]. Molecular oxygen found in the aqueous solution was utilized to initiate catechol autoxidation and generated H_2O_2 as a byproduct. The generated H_2O_2 was found to disinfect both gram negative and positive bacteria as well as various viruses, including the chemical resistant, non-enveloped porcine parvovirus (PPV) [40, 42]. However, our prior work required fully submerging the catechol-containing biomaterial into an aqueous solution to oxidize catechol for generating sufficient amounts of H_2O_2 for disinfecting pathogens. The limited moisture content in respiratory droplets, compared to fully submerging a material, could potentially restrict the amount of H_2O_2 generation needed to achieve satisfactory pathogen disinfection.

To utilize the limited amount of moisture in the respiratory droplets to oxidize catechol to generate antipathogenic levels of H_2O_2, it is necessary to tune the reactivity of catechol to promote faster auotoxidation. Catechol functionalized with electron withdrawing groups such as a nitro group ($-NO_2$) have been previously found to have increased resistance to autoxidation (Figure 1) [44, 45]. Similarly, catechol modified with electron withdrawing halogenated atoms (e.g., Cl, Br, and I) generates significantly less H_2O_2 when compared to that of unmodified catechol [46]. On the contrary, catechol modified with an electron donating hydroxyl (-OH) group demonstrated decreased resistance to oxidation when compared to unmodified catechol [47]. Thus, we hypothesize that -OH group-modified catechol can be utilized to create a surface coating with increased rate of autoxidation and H_2O_2 generation. Generation of H_2O_2 through the autoxidation of 6-hydroxydoapmine has also been previously reported [48, 49].

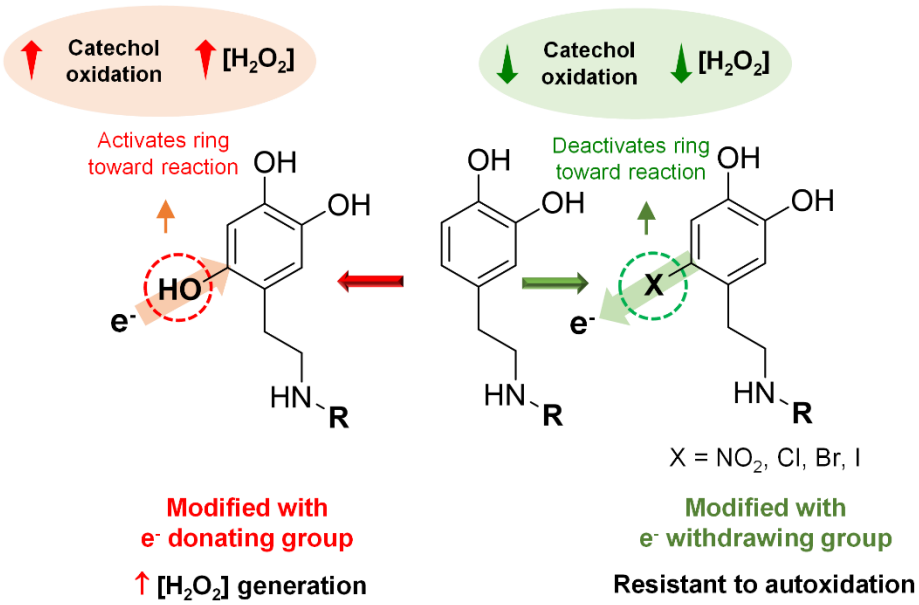

Figure 1. Chemical structures of catechol side chain of dopamine can be modified with electron donating and electron withdrawing groups to tune its autoxidation rate. Modification with electron donating -OH group is expected to increase the rate of autoxidation and H_2O_2 generation.

To this end, we created a polymer incorporated with 6-hydroxydopamine (6-OHDA), a catechol modified with -OH group at the 6-position of the benzene ring. The ability for 6-OHDA to generate H_2O_2 upon hydration was evaluated and compared with that of dopamine with unmodified catechol. Catechol-containing polymers were coated onto melt-blown nonwoven polypropylene (PP) fabric typically used in face masks. The ability of the coated PP fabric to rapidly generate antipathogenic levels of H_2O_2 for disinfecting model respiratory viruses (bovine viral diarrhea (BVDV) and human coronavirus 229E (HCoV 229E)) and bacteria (*Staphylococcus aureus*, *Staphylococcus epidermidis*, *Pseudomonas aeruginosa*, and *Escherichia coli*) was investigated.

2. Materials and Methods

2.1. Materials

Acrylamide (AAm), 6-hydroxydopamine hydrochloride (6-OHDA), 2,2′-azobis(2-methylpropionitrile) (AIBN), 4-methylmorpholine, dimethyl sulfoxide (DMSO), dimethyl sulfoxide-d6 (DMSO-d_6), and *N*,*N*′-dimethylformamide (DMF) were purchased from Sigma-Aldrich (St Louis, MO). Acrylic acid *N*-hydroxysuccinimide (AA-NHS) was purchased from ACROS Organics (Fair Lawn, New Jersey). Phosphate-buffered saline (PBS), ethyl acetate (EA), ethanol, and isopropyl alcohol (IPA) were purchased from Fisher Scientific (Pittsburg, PA). Pierce Quantitative Peroxide Assay Kit (FOX assay) (Thermofisher scientific), eagle's minimum essential media (EMEM), fetal bovine serum (FBS), sodium pyruvate, non-essential amino acid (MEM NEAA), Dulbecco's Eagle's minimum essential media (DMEM), and horse serum albumin (HAS) were purchased from Thermofisher Scientific (Rockford, IL). PP mask material was purchased from Sailrite (Columbia City, IN). Tryptic soy broth (TSB), Mueller Hinton agar (28 mL fill, 15 × 100 mm), and astral inoculation loop (10 μL, sterilized) were purchased from Hardy Diagnostics (Santa Maria, CA). *S. aureus* (ATCC 43300), *P. aeruginosa* (ATCC 27318), *S. epidermidis (*ATCC 12228), *E. coli* (ATCC 11229), human lung fibroblast (MRC-5, ATCC), BVDV (ATCC VR-1422), and bovine turbinate cells (BT, ATCC CRL 1390) were obtained from American Type Culture Collection (ATCC, Manassas, Virginia). HCoV 229E (NIH: NR-52726) was received from BEI Resources. 2-(3,5-diphenyltetrazol-2-ium-2-yl)-4,5-dimethyl-1,3thiazolebromide (98%, MTT) was purchased from Alfa Aesar (Haverhill, MA), bovine liver catalase (2000-5000 U/mg), and sodium dodecyl sulfate (SDS, BioReagent, ≥98.5%) was purchased from Sigma Aldrich (St Louis, MO). Normal Human Immortalized Keratinocyte cells (HaCaT) were obtained from Addexbio Technologies© (T0020001). Dopamine methacrylamide (DMA) was prepared following a previously published protocol [50].

2.2. Synthesis of Polymers

6-OHDA modified polymer was prepared in two steps (Figure 2). First, AA-NHS (0.55 g, 3.25 mmol) and AAm (0.91 g, 13 mmol) were dissolved in DMSO (20 mL), and AIBN (0.02 g) was then added to the reaction mixture under nitrogen. The reaction mixture was frozen for 30 minutes, degassed three times by backfilling with nitrogen, and stirred for 3 h at 75 ˚C. The polymer was precipitated in EA, washed with EA, and dried under vacuum. In the second step, the AA-NHS containing polymer (0.4 g, 0.25 mmol) was dissolved in DMSO (20 mL) while stirring (500 rpm) at 70 ˚C. The reaction mixture was allowed to equilibrate at room temperature (RT) and then 4-methylmorpholine (108 µL, 0.25 mmol) was added with a syringe under a stream of nitrogen while magnetically stirring at 500 rpm. 6-OHDA (0.304 g, 0.375 mmol) was dissolved in DMSO (5 mL) and added to the reaction mixture with a syringe under nitrogen.

To prepare the polymer with unmodified catechol, DMA (0.110 g, 0.5 mmol) and AAm (0.355 g, 5 mmol) were dissolved in DMF (2 mL) under nitrogen and AIBN (0.005) was added. The reaction mixture was magnetically stirred (500 rpm) for 3 h at 70 ˚C. The reaction mixture was precipitated in EA, washed with EA, and vacuum dried. Polyacrylamide was utilized as the catechol-free control and was synthesized by dissolving AAm (2 g) and AIBN (0.023 g) in DMSO (20 mL) under nitrogen while magnetically stirring at 40 ˚C for overnight. The polymer was precipitated in EA, washed with EA, and vacuum dried. 6-OHDA modified polymer, DMA modified polymer, and polyacrylamide were denoted as DAOH, DA, and A, respectively (Figure S1).

Proton nuclear magnetic resonance (^{1}H NMR) spectroscopy (500 MHz, Bruker) was used to analyze the chemical composition of the as-prepared polymers. Catechol content in these polymers was determined using UV-Vis spectroscopy (LAMBDA35, PerkinElmer, MA) with standard curves prepared using solutions of either 6-DAOH or dopamine. Fourier transformed infrared

spectroscopy (FTIR, PerklinElmer Spectrum One) was performed on dried polymers. A gel permeation chromatography (GPC, Shimadzu HPLC Nexera Series) system equipped with a UV detector (SPD-40, Shimadzu), a refractive index detector (RID-20A, Shimadzu), and a multiple-angle light scattering detector (miniDAWN, Wyatt) was used to determine the number average molecular weight (M_n), the weight average molecular weight (M_w), and the polydispersity index (PDI) of the polymers. 20 µL of polymer solution (5 mg/mL in DMSO) was injected and eluted at 0.5 mL/min through a Shodex OHpak LB-803 column using DMF (HPLC grade) as the mobile phase while keeping the column in an oven at a temperature of 40°C.

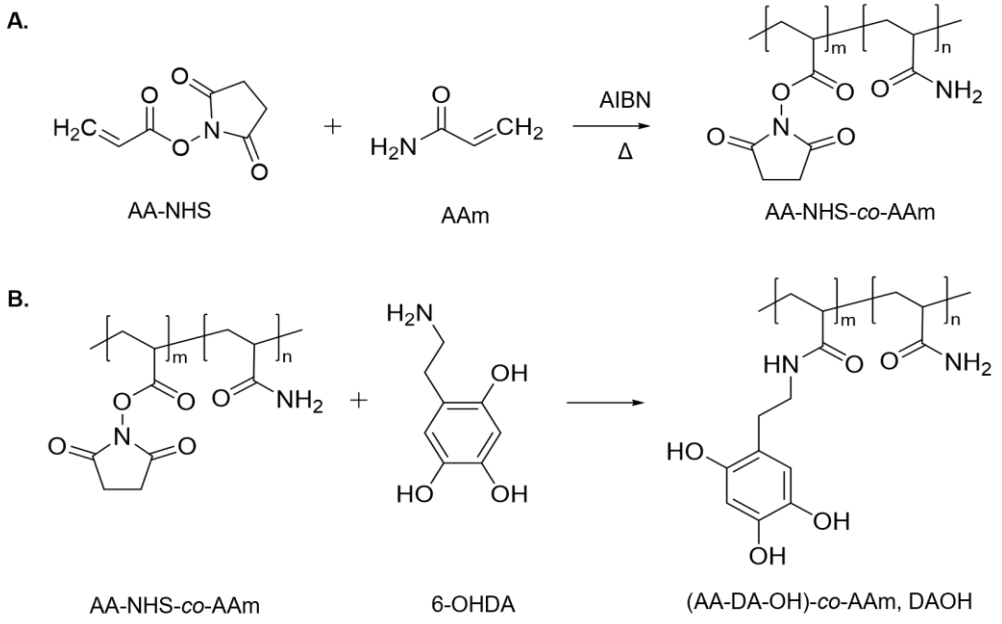

Figure 2. Synthesis of 6-OHDA modified polymer, DAOH. (A) AAm was polymerized with AA-NHS that contains NHS-activated ester. (B) 6-OHDA was further reacted with AA-NHS-co-AAm to obtain DAOH as the final product.

2.3. Preparation of Self-Disinfecting Coatings on the PP Fabrics

A 5 wt% polymer solution in DMSO was dropped onto PP fabrics wetted with DMSO. The volume of the polymer solution was adjusted to obtain 30 and 40 wt% polymer coatings on the

fabric relative to the mass of PP. Fabrics were then wrapped with aluminum foil and left for 1 h to let the solution penetrate the fabric completely and then dried under vacuum at RT overnight. Polymer-coated fabrics were then washed with IPA and vacuum dried. Polymer-coated PP fabrics were given a name that consisted of a number 30 or 40 corresponding to the wt% of the polymer followed by the name of the polymer coating (Table 1). For example, fabric coated with 30wt% DAOH was denoted as 30DAOH.

Table 1. List of polymer coatings on the PP fabric and corresponding abbreviations.

Polymer Coatings on PP Fabric	Abbreviation
Uncoated PP fabric	PP
30 wt% AAm	30A
40 wt% AAm	40A
30 wt% DMA-co-AAm	30DA
40 wt% DMA-co-AAm	40DA
30 wt% (AA-DA-OH)-co-AAm	30DAOH
40 wt% (AA-DA-OH)-co-AAm	40DAOH

2.4. Characterizations of Polymer-coated PP Fabrics

FTIR spectroscopy was performed on the uncoated and polymer-coated PP fabrics. Environmental scanning electron microscopy (ESEM, Philips XL 40) and energy-dispersive spectroscopy (EDS) were employed to evaluate the morphology and elemental distribution of the polymer-coated PP fabrics. The uncoated and polymer-coated fabrics were coated with Pt/Pd sputter coating with a thickness of 5 nm, mounted using the double-sided carbon conducting tape on the aluminum stub. The images were taken using the voltage of 5 kV and working distance of 10 mm.

The porosity of the polymer-coated PP was evaluated using the *n*-butanol uptake method [51], where the porosity (P) was determined by immersing the dry fabric in *n*-butanol for 1 h. P was calculated using the following equation.

$$P(\%) = \frac{M_{BuOH}/\rho_{BuOH}}{M_{BuOH}/\rho_{BuOH} + M_p/\rho_P} \times 100 \quad (1)$$

where, M_{BuOH} is the mass of the absorbed *n*-butanol, ρ_{BuOH} is the density of n-butanol, M_p is the mass of the dry PP fabric, and ρ_P is the density of the polymer.

The contact angle measurement was performed using a contact angle goniometer (Ossila Contact Angle Goniometer). A 5 μL droplet of deionized (DI) water was placed onto the surface of PP fabrics from a height of 10 mm. After the droplet was allowed to equilibrate, an image was captured. The contact angle was measured by considering both sides of the droplet.

The stability of DAOH and DA coatings was investigated by soaking the coated PP fabric swatches (radius = 12.5 mm) in DI water for 24 hours. UV-Vis spectroscopy was used to quantify the concentration of DAOH and DA leached from the coatings at specific time points. Additionally, we subjected the DAOH and DA coatings (r = 10 mm) to forcibly wrinkling and rubbing against themselves for ~ 20 seconds (Video S1). The H_2O_2 generation from the fabrics using 2 mL pH 7.4 PBS was determined before and after the rubbing process.

2.5. Determination of H_2O_2 Concentration

Polymer-coated and uncoated PP fabrics (1×1 cm) were hydrated with a drop of 100 μL of pH 7.4 PBS and incubated at room temperature (RT) and 37 ˚C. At a given time point, the H_2O_2 concentration was quantified using Pierce Quantitative Peroxide Assay Kit following a published protocol [43]. H_2O_2 solutions with concentrations ranging from 0 to 1 mM was prepared to create a

standard curve. The experiment was performed in triplicate and the results are presented as the mean ± standard deviation.

2.6. Antibacterial Activity of Polymer-coated PP Fabrics

The antibacterial activity of the polymer-coated PP fabrics was evaluated against both Gram-positive (*S. aureus* and *S. epidermidis*) and Gram-negative (*P. aeruginosa* and *E. coli*) bacteria following a published protocol with minor modification [52]. Frozen bacteria were hydrated with TSB and then isolated in an agar plate. A single bacteria colony was used to inoculate 5 mL of TSB. The bacteria culture was sealed and incubated at 37 ˚C with gentle agitation (50 rpm) for 24 h. The bacteria culture was diluted to 10^6 cfu/mL using sterile PBS (pH 7.4) and the cell concentration was determined using UV-Vis turbidity measurements at 600 nm. Uncoated and polymer-coated PP fabrics were cut to the dimension of 1×1 cm, placed in a 24-well cell culture plate, and sterilized by UV irradiation for 15 min. A single 100 µL drop of bacteria suspension was applied onto the surface of each fabric. The 24-well plate was sealed with parafilm and kept at either RT or 37 ˚C. At a given time point, 10 µL of the bacteria solution was pipetted out without touching the fabric and streaked with the sterile loop onto the agar plate. Agar plates were incubated at 37 ˚C for 24–48 h. Bacteria colonies grown on the agar plates were photographed and counted using ImageJ. The relative colony number was calculated using the following equation [53].

$$\text{Relative colony number (\%)} = \frac{N_m}{N_p} \times 100\% \quad (2)$$

where N_m represents the number of colonies formed when bacteria were exposed to the fabrics and N_p represents the number of colonies formed when bacteria were exposed to PBS without the presence of fabrics. The experiment was performed in triplicate and the results are presented as the mean ± standard deviation.

The bacteria inhibition kinetics data was determined using a first order rate (r) model as described by the following equation.

$$r = \frac{dN}{dt} = k \times N \quad (3)$$

where N represents the bacteria colony numbers, t is the time in hours, and k is the first order rate constant in s^{-1}. Data points from the first 3 hours were used for each bacteria strain. The slope of each data set was determined to get an average and standard deviation for the k value.

Morphologies of bacteria after exposure to the uncoated and polymer-coated PP fabrics were imaged using a field emission scanning electron microscope (FE-SEM, Hitachi S-4700). To prepare the samples for imaging, UV-sterilized PP fabrics (1×1 cm) were placed in 24-well cell culture plates with 500 μL of bacteria suspension (10^6 cfu/mL). The well plates were sealed with parafilm and incubated at 37 °C for 6 h. The PP fabrics were washed with PBS, and fixed with 2.5% glutaraldehyde solution overnight at 4 °C. The fabrics were washed with PBS and dehydrated through successive treatments using 30, 50, 70, 80, 90, 95, and 100% ethanol for 30 min during each treatment. Finally, the fabrics were freeze-dried overnight.

2.7. Antiviral Activity of Polymer-coated PP Fabrics

BVDV and HCoV 229E were used to evaluate the antiviral activity of polymer-coated PP fabrics following previously published protocols with minor modification [40]. Prior to virus treatment, circular swatches of the PP fabrics were cut to fit the wells of a 24-well cell culture plate and disinfected by UV for 15 minutes in a laminar flow hood. Following disinfection, a single 150 μL drop of at least 6 $\log_{10}MTT_{50}$/mL solution of BVDV or HCoV was applied to the fabrics and incubated for up to 24 h. Following incubation, the treated virus droplet was carefully recovered and titrated using a colorimetric cell viability assay, the MTT assay, as described earlier [54, 55].

Briefly, BT and MRC-5 cells were seeded at a cell density of 2×10^4 cells/well and 1×10^4 cells/well, respectively, in a 96-well plate for 12-24 h. BT and MRC-5 are used as the indicator cells for BVDV and HCoV 229E, respectively. Virus supernatant (25 µL) was added to the wells in quadruplicate, with a serial dilution of 1:5 across the plate. After incubating the plates for 6 days at 37 ˚C for BT and 35 ˚C for MRC-5, 10 µL of MTT solution at a concentration of 5 mg/mL of MTT in PBS (pH 7.2) was added to each well and incubated for 4 h. After 4 h, 100 µL of 10% SDS at a pH of 2 was added to each well as a solubilization buffer. After 4-24 h, the absorbance was determined using a Synergy Mx microplate reader (BioTek, Winoski, VT) at 550 nm. The 50% infectious dose of the virus was determined by finding the concentration where 50% of the cells were viable, labeled the MTT_{50}. Log reduction values (LRVs) were calculated using the following equation.

$$\mathrm{LRV} = -\log\left(\frac{C_i}{C_f}\right) \tag{4}$$

where C_i is the initial concentration of virus and C_f is the final concentration of virus after treatment. The inactivation kinetics data was determined using Equation (3) while using $\log_{10}$ MTT_{50}/mL values as N.

2.8. Cytotoxicity Assays

Immortalized human keratinocyte cells (HaCaT) were used to evaluate the cytotoxicity of the polymers and polymer-coated fabrics with and without bovine liver catalase (1 mg/mL). To assess the cytotoxicity of the polymers, 96-well plates were coated with 100 µL of polymer solution (10% in DMSO) and dried under vacuum conditions overnight. To assess the cytotoxicity of the PP polymer-coated fabrics, fabrics were cut into swatches matching the size of 48-well plates (radius = 0.23 cm) and placed at the bottom of the well. The well plates were sterilized using UV irradiation for 30 minutes. After sterilization, HaCaT cell solutions with and without catalase were

added to the well plates at a density of 20,000 cells/cm² and incubated for 48 hours. Cell viability after 48 hours was assessed using the Resazurin assay following a published protocol [56]. The results were normalized based on the cell viability for cells seeded in polystyrene tissue culture wells.

2.9. Statistical Analysis

One-way analysis of variance (ANOVA) with the Tukey method was used for comparing means of multiple groups using a *p*-value of 0.05.

3. Results and Discussion

3.1. Preparation of Coatings on PP Fabrics

Polyacrylamide grafted with either unmodified dopamine (DA) and 6-OHDA (DAOH) were prepared (Figure S1). Catechol-free polymer (A), which does not release H_2O_2, was synthesized and utilized as the control. The composition of the polymers was confirmed using ^{1}H NMR (Figures S2-S4) and UV-vis spectroscopy (Figures S5 and S6). NMR spectrum for DAOH exhibited 2 benzyl protons (6.30 and 6.39 ppm) as opposed to 3 protons found in the unmodified catechol. UV-Vis spectrum of DAOH exhibited a maximum wavelength (λ_{max}) at 300 nm, corresponding to the 6-OHDA which is shifted from unmodified catechol with a λ_{max} of 285 nm. Catechol content of DAOH and DA were determined to be 27.8 mol% and 16.1 mol%, respectively. FTIR spectra of the polymers confirmed the characteristics peaks for AAm (–NH_2 3450–3050 cm^{-1}, C═O 1650 cm^{-1}) and catechol (–OH, 3450–3050 cm^{-1} and benzene rings 1600–1500 cm^{-1}) (Figure S7).

GPC was utilized to determine the molecular weights of the synthesized polymer (Table 2). DA exhibited M_n and M_w values that were an order of magnitude lower when compared to those of A and DAOH. DA was directly synthesized through free-radical polymerization of DMA with AAm. Catechol is known to inhibit and retard free-radical polymerization in the presence of molecular

oxygen [57, 58]. Although the synthesis of DA was carried out in a nitrogen-rich environment, the presence of catechol likely affected its extent of polymerization. On the contrary, DAOH was synthesized in 2 steps where the 6-hydroxydopamine is coupled to AA-NHS-co-AAm after the formation of the polymer. As such, the extent of polymerization was not affected. However, copolymerization between AAm and AA-NHS resulted in higher PDI when compared to the synthesis of A, a homopolymer.

Table 2. Molecular weights of polymers based on GPC analysis.

Polymer	Mn (g/mol)	Mw (g/mol)	PDI
A	4.37×10^6	5.51×10^6	1.26
DA	1.38×10^5	4.37×10^5	3.17
DAOH	1.05×10^6	4.24×10^6	4.02

Catechol-containing polymers were then coated onto melt-blown PP fabric (Figure S8), commonly used in the production of face masks that do not have intrinsic antiviral and antibacterial properties. FTIR spectra of uncoated and polymer-coated PP fabrics demonstrated peaks between 2,750 and 3,000 cm^{-1}, which is attributed to C-H bands found in PP. Additionally, polymer-coated fabrics exhibited peaks associated with AAm ($–NH_2$ 3450–3050 cm^{-1}, C═O 1650 cm^{-1}) while DA and DAOH exhibited peaks associated with and catechol (1,309, 1,521, and 1,657 cm^{-1} attributed to C–N stretching of the indole ring, C=N of indole amine, and C=C of the benzene ring and C-H bands of PP fabric, respectively) (Figure S9). From ESEM images and EDS mapping analysis, the polymer-coated PP fabric maintained the desired porous structure (Figure 3). The polymer coating appears to distribute evenly throughout the fabric based on the presence of nitrogen (N) and oxygen (O) atoms (Figure 3). The PP fabric consists of only carbon (C) and hydrogen (H) atoms and the

addition of DAOH and DA polymers contributed to the observed N and O atoms found on the polymer-coated fabrics.

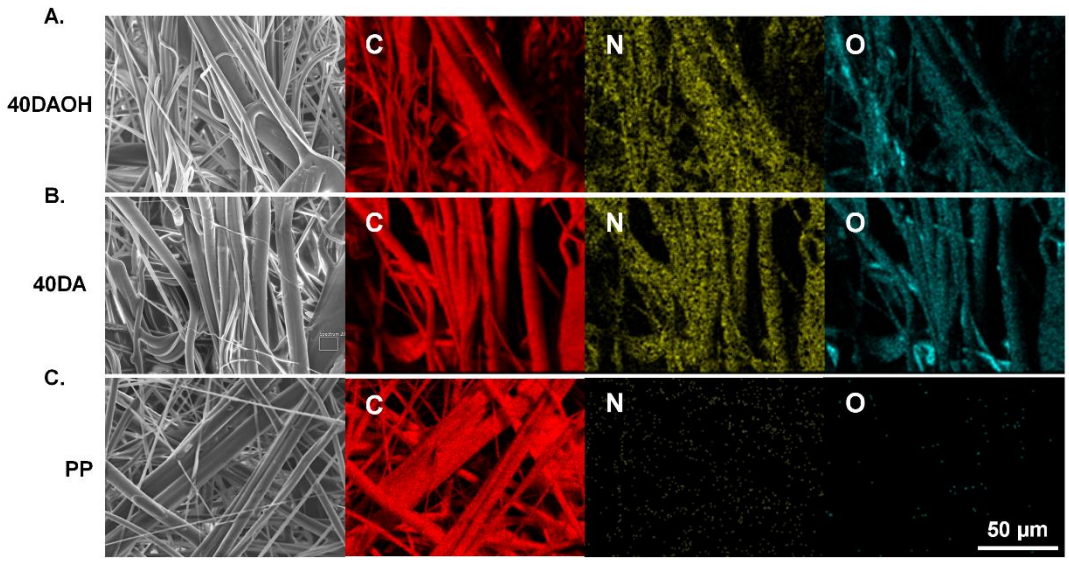

Figure 3. ESEM images and EDS maps of (A) 40DAOH, (B) 40DA, and (C) uncoated PP fabrics. Carbon, nitrogen, and oxygen atoms are shown in red, yellow, and blue, respectively.

The porosity of the polymer-coated PP averaged around 80% regardless of the polymer type (Table S1). Porosity of the PP fabric is a characteristic property crucial to maintaining filtration efficiency and breathability of a facemask. Although the porosity of the coated PP decreased slightly when compared to the uncoated fabric (86%), porosity of polymer-coated PP still exceeded the known values for surgical (77%) and N95 (65%) masks [59].

The uncoated PP fabric was relatively hydrophobic with a water contact angle of 144˚ (Table 3, Figure S10). Water contact angle decreased with the application of the polymer coating, which further decreased with increasing coating content. DAOH, DA, and A polymer coatings displayed relatively hydrophilic properties, potentially due to the presence of the hydrophilic polyacrylamide backbone and -OH groups found in catechol. This increase in the hydrophilic nature of the polymer coated fabric is desirable as it will increase the ability for the coating to absorb moisture and

generate H_2O_2. The decrease in hydrophobicity directly contributes to reduced droplet drying time [60] and the formation of daughter droplets [61].

Table 3. Water contact angle of uncoated and polymer-coated PP fabrics.

Sample	Contact Angle (°)
Uncoated PP fabric	144.12 ± 1.52
30A	117.85 ± 4.37
40A	113.39 ± 4.62
30DA	138.13 ± 6.29
40DA	124.19 ± 5.62
30DAOH	136.10 ± 5.65
40DAOH	125.12 ± 1.72

3.5. Determination of H_2O_2 Concentration

PP fabrics were hydrated by a single drop of PBS (pH 7.4) and incubated at RT or 37 ˚C, and the effect of catechol modified with electron donating -OH group on H_2O_2 generation from polymer-coated PP fabrics was evaluated (Figure 4). Upon hydration, the DAOH-coated PP fabrics (30DAOH and 40DAOH) generated 1,000 to 3,000 μM of H_2O_2 within 1 h, which is more than 3 orders of magnitude higher than PP fabrics coated with polymers that contained unmodified catechol (30DA and 40DA). H_2O_2 generated from 30DAOH and 40DAOH continued to increase and approached a maximum of nearly 4,000 μM within 24 h. On the other hand, 30DA and 40DA only generated a maximum of 1,500 μM after 24 h. DAOH generated a significantly higher amount of H_2O_2 and at a faster rate when compared to DA due to the presence of the electron donating -OH group which enabled fast catechol oxidation upon hydration. PP coated with higher polymer content (i.e., 40wt%) also generated higher amounts of H_2O_2 regardless of coating composition. This indicated that the higher amount of catechol and 6-OHDA contributed to higher levels of

H_2O_2 generation. Similarly, higher levels of H_2O_2 was measured at 37 ˚C when compared to RT, due to increased catechol oxidation rate at an elevated temperature [36]. Both the control polymer-coated (30A and 40A) and the uncoated PP fabric did not generate any H_2O_2.

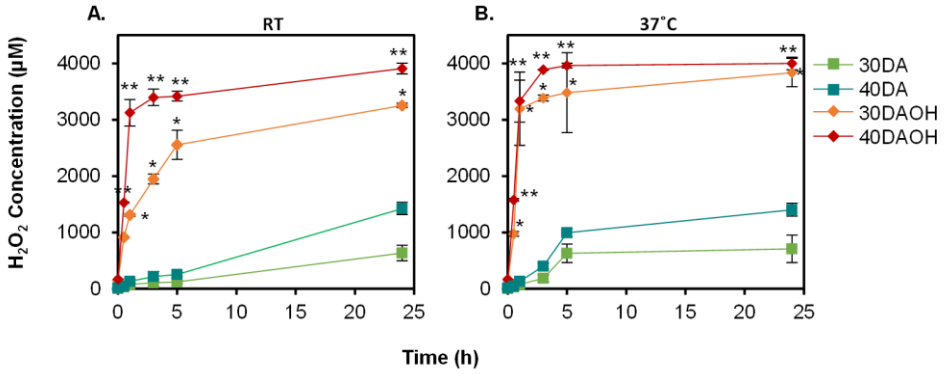

Figure 4. H_2O_2 generated from DA- and DAOH-coated PP fabrics when incubated with 100 µL of pH 7.4 PBS at (A) RT and (B) 37˚C. *$p < 0.05$ when compared to the control coating at the same time point. **$p < 0.05$ when compared to the DA coating at the same time point. ($n = 3$).

To showcase the coating's rapid H_2O_2 production upon hydration through small water droplets, we sprayed a mixture of PBS and the FOX assay reagent onto the surface of the DAOH-coated PP fabric (Video S2). The color of these droplets changed to purple in less than a minute, indicating the generation of H_2O_2 when the coating is hydrated. This video indicated that the polymer-coated fabric can be activated when hydrated using small water droplets with diameters under 1 mm. The ability to activate H_2O_2 using water droplets less than 1,000 µm indicates the potential to activate the coating utilizing respiratory droplets which are reported to have diameter of 5 to 1,000 µm [3, 4].

3.6. Stability of the Polymer-Coating

To assess the coating stability, we used two methods: (1) submerging the coated PP-fabrics in DI water to evaluate the amount of polymer released into the aqueous solution and (2) mechanically wrinkling and rubbing the coated fabrics and evaluate its effect on the ability of the

coated fabric to generate H_2O_2. When 40DAOH and 40DA were submerged in DI water, the coated polymers gradually leached into the aqueous solution over 24 hours (Figures S11 and S12). However, only a very small amount of the coated polymer (<1.2 wt%) was detached over this time period (Tables S2 and S3). This indicated that the coatings are relatively stable toward submersion in water. Although these polymers are soluble in polar organic solvents, they are insoluble in water.

The PP fabrics are intended to function as a filter for a respirator which will not be fully submerged in an aqueous solution. As such, polymer-coated were further subjected to mechanical wrinkling and rubbing (Video S1). These coated fabrics were permanently wrinkled after the rubbing treatment (Figure S13). For 40DAOH, there was no difference in the amount of H_2O_2 generation after the fabric was subjected to rubbing (Figure S14). However, 40DA generated significantly lower amount of H_2O_2 generation. The elevated molecular weight of DAOH likely contributed to the enhanced stability of the coating when compared with DA.

3.7. Antibacterial Activity of Polymer-coated PP Fabrics

The antimicrobial activity of the polymer-coated PP fabrics was evaluated using both Gram-positive (*S. aureus and S. epidermidis*) and Gram-negative (*P. aeruginosa and E. coli*) bacteria at a starting concentration of 10^6 cfu/mL (Figures 5 and S15). All 4 bacteria strains were chosen due to their potential in causing respiratory infections [62-64]. Over time, the number of colonies formed decreased for both DAOH- and DA-coated PP fabrics. However, the DAOH-coated PP fabric exhibited significantly better antibacterial activity, resulting in a near complete reduction in the relative colony number within 3-5 h for all 4 bacteria strains (Figure S15). Conversely, DA-coated PP fabrics required nearly 24 h to achieve similar results. This result demonstrated the impact of adding the electron donating -OH group to the catechol side chain in enhancing H_2O_2 generation and antibacterial activity. PP coated with a higher polymer content also demonstrated better

antibacterial results due to higher H_2O_2 generation. The antibacterial activity was increased at 37 ˚C when compared to RT. At an elevated temperature, a significantly higher amount of H_2O_2 was generated, which contributed to a better antibacterial performance. The uncoated PP fabric and A-coated fabric did not show antibacterial activity compared to the initial bacteria solution.

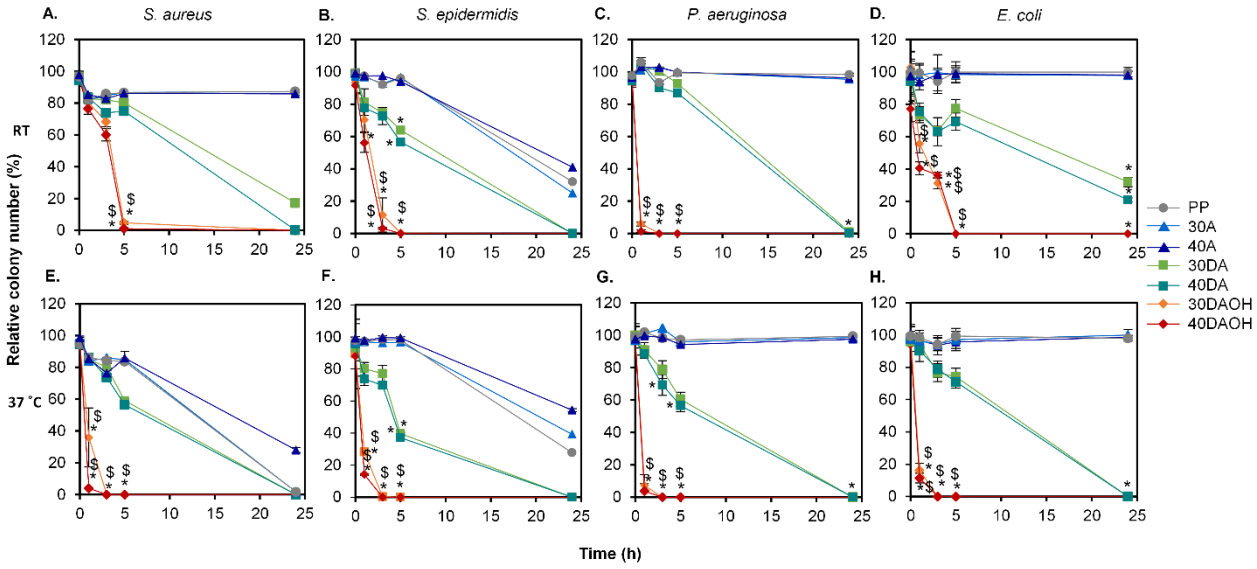

Figure 5. The relative bacteria colony number for (A and E) *S. aureus*, (B and F) *S. epidermidis*, (C and G) *P. aeruginosa*, and (D and H) *E. coli* exposed to PP fabrics at (A-D) RT and (E-F) 37 ˚C. The relative colony number was normalized by the number of colonies formed by the bacteria not exposed to the fabrics. *$p < 0.05$ when compared to the control coating and uncoated PP fabrics at the same time point. $^{\$}p < 0.05$ when compared to the DA-coated PP fabrics at the same time point. (n = 3).

The first order inactivation constant (k) was calculated based on the bacteria colonies determined for the first 3 h of antibacterial tests for all 4 strains of bacteria (Figures S16-S23 and Tables S4 and S5). k values for the DAOH coating were significantly higher for all four bacteria strains when compared to those calculated for DA coatings (Figure 6). In some instances, k values for DAOH

were 1-2 orders of magnitude higher when compared to DA. However, there were no significant differences between 30DAOH and 40DAOH coatings and between 30DA and 40DA coatings. In general, k values were higher for experiments performed at 37 ˚C when compared to values calculated for RT for DAOH-coated fabrics. A faster rate of H_2O_2 generation at 37 ˚C likely contributed to the increased k values. Additionally, it is suboptimal for culturing these four strains of bacteria at a lower temperature, which may affect their inhibition rates differently [65-68]. At room temperature, higher k values were observed for *P. aeruginosa* and *S. epidermidis* when compared to the other two strains. For *P. aeruginosa*, temperature changes greatly affect the activation of virulence pathways, which is inactive below 30°C [67]. On the other hand, *S. epidermidis* exhibits a high capability for surface adherence, making the coating a preferred material for this strain [69].

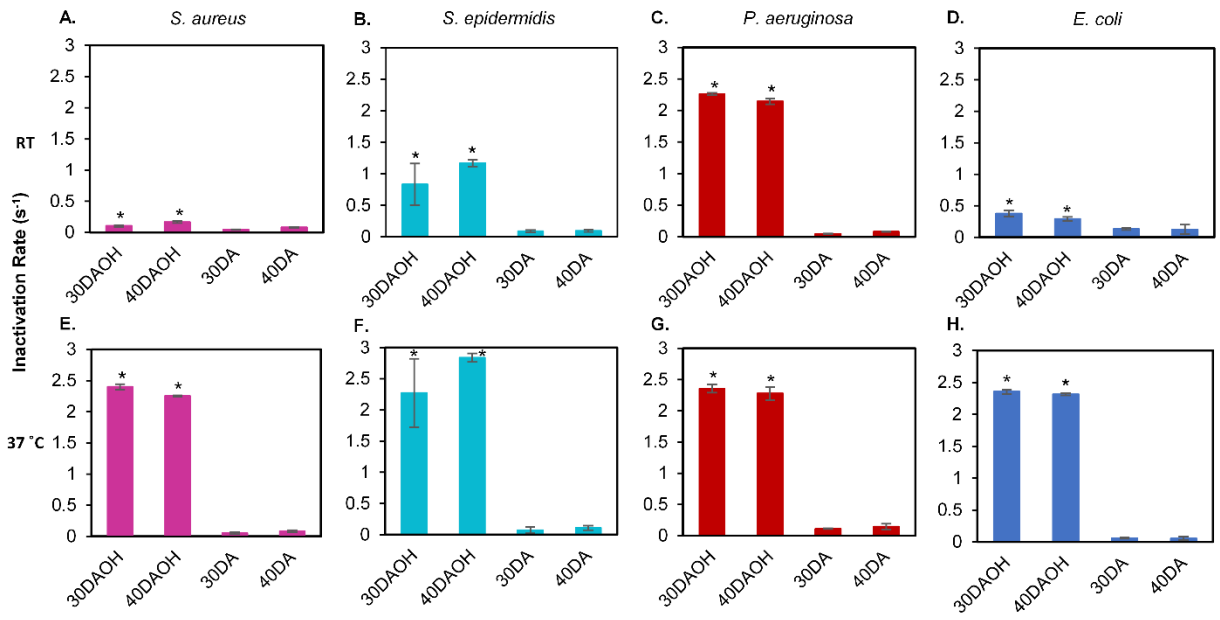

Figure 6. First order rate constant of inactivation for (A and E) *S. aureus*, (B and F) *S. epidermidis*, (C and G) *P. aeruginosa*, and (D and H) *E. coli* for DAOH and DA coatings determined at (A-B) RT and (E-H) 37 ˚C. *p < 0.05 when compared to the DA coating with the same coating weight percent. (n = 3).

The morphology of the bacteria was visualized using FE-SEM (Figure 7). Bacterial strains that were not exposed to the fabrics exhibited intact cell walls and well-defined morphology. Similarly, bacteria that were exposed to the control fabrics (PP and A) exhibited intact cell walls and morphology that was similar to those found in the bacteria pellet. However, bacteria exposed to H_2O_2-releasing DAOH and DA coatings completely lost their morphological, structural, and cellular integrity, leading to cellular lysis. With DAOH coatings, some cells were completely decomposed, leaving only traces of the cell membranes visible. Cells exposed to DA coatings experienced severe disruption followed by cellular lysis. These significant morphological changes are attributed to the potent oxidizing properties of H_2O_2. These results align with previous studies where bacteria treated with H_2O_2 exhibited similar morphological changes [70-75].

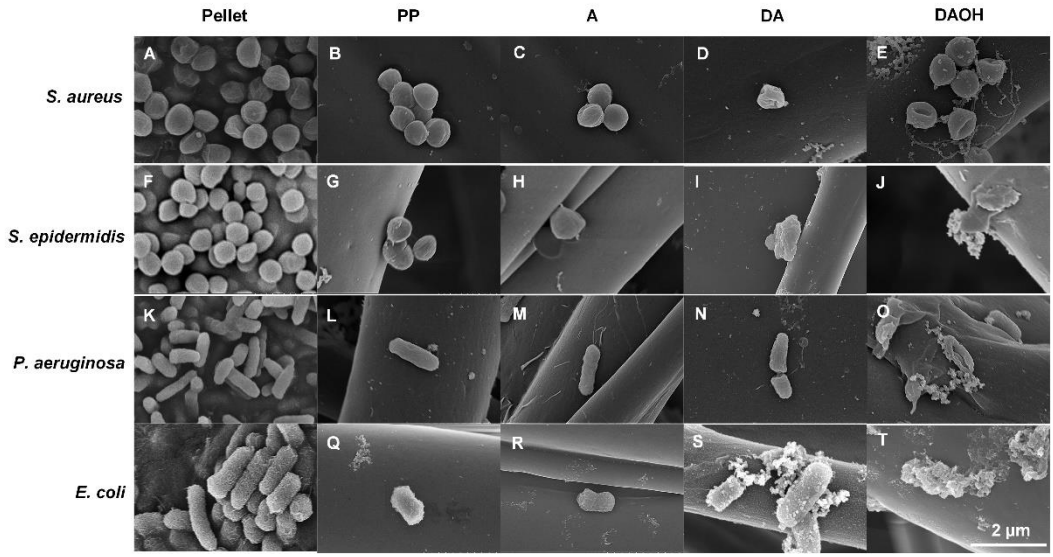

Figure 7. FE-SEM images of (A-E) *S. aureus*, (F-J) *S. epidermidis*, (K-O) *P. aeruginosa*, and (P-T) *E. coli* when exposed to uncoated and polymer-coated PP fabrics.

3.8. Antiviral Activity of Polymer-coated PP Fabrics

The virucidal activity of polymer-coated PP fabrics was evaluated using two model viruses, BVDV and HCoV 229E. BVDV was chosen because our team has previously studied the inactivation of this virus using catechol-containing microgels that releases H_2O_2 [40, 42]. On the other hand, HCoV 229E is a human coronavirus that transmits via droplet-respiration and fomites, and is a model virus for SARS-CoV-2 that resulted in COVID-19 pandemic [76]. Both 30DAOH and 40DAOH showed a 2.2 log reduction in the titer of BVDV after incubation for 24 h at RT (Figure 8). This corresponds to a 99.4% reduction in the viral load. Uncoated PP fabric, 30A, and 40A did not show virucidal activity over the same time period. Although both 30DA and 40DA generated H_2O_2, the amount generated was not virucidal against BVDV. This further highlights the need for the -OH modified catechol to achieve sufficient antiviral behavior.

HCoV 229E was unstable when added to the PP surface and self-inactivated within 24 h (Figure 8C and 8D). While the stability of HCoV on surfaces for up to 6 days is reported in the literature, the characteristics of the surface greatly influence virus persistence [77]. Melt-blown PP is hydrophobic with high filtration efficiency and may accelerate virus inactivation or interfere with virus recovery [78]. In 6 h, 30DAOH and 40DAOH exhibited around 2.5 log reduction in the titer of HCoV corresponding to > 99.7% reduction of the viral load. This reduction in the titer value is significantly higher when compared to the control surfaces which demonstrated only 1.1 log reduction over 6 h. After 24 h, the titer of HCoV reduced to the limit of detection values with both the control and catechol-containing coatings. The reduction in virus titer may be due to the interaction between the fabric or incomplete recovery of virus solution from the fabric following incubation. A similar observation was reported for the inactivation of HCoV contacting quaternary ammonium compound functionalized PP fabric where a reduction in HCoV titer was observed despite a lack of virucidal activity [12]. While the results indicate that HCoV can be self-inactivated,

DAOH-coated fabrics were able to accelerate this inactivation process. It is also important to note that the active virucidal ingredient, H_2O_2 was cytotoxic to MRC5 cells, the indicator cell line utilized in assessing HCoV infectivity (Figure S24). As a result, it is possible that the virus inactivation could be higher than what was observed, but due to an increase in the limit of detection of the MTT assay, lower log reduction values had to be reported.

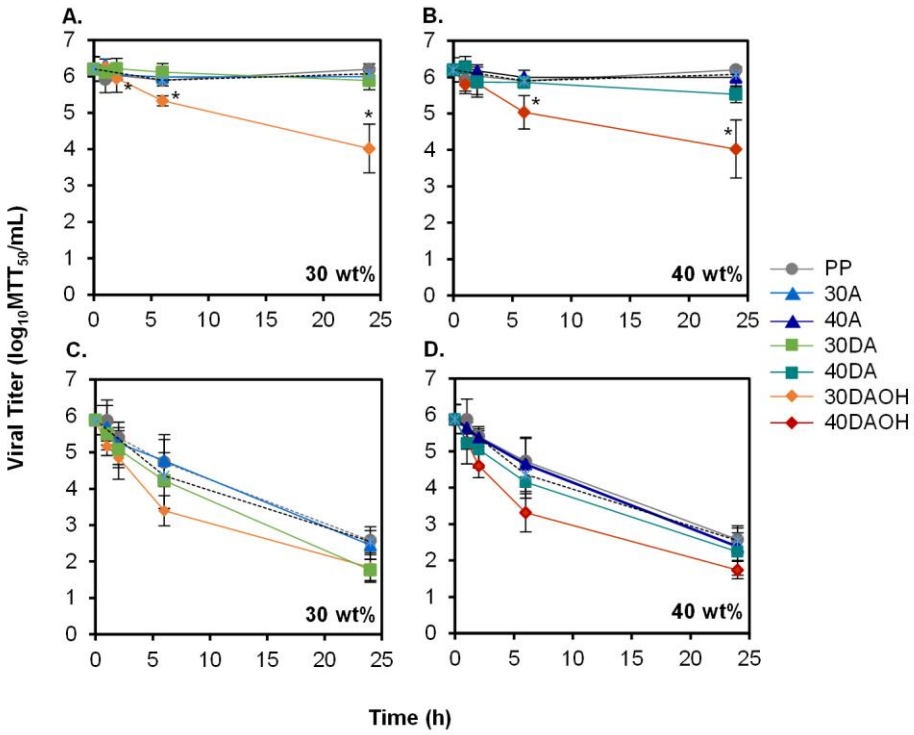

Figure 8. Time-dependent inactivation of (A and B) BVDV and (C and D) HCoV 229E. A drop of crude virus solution (BVDV or HCoV) was incubated with PP and DAOH- and DA-coated PP fabrics at RT. The dashed line in black represents virus control. *$p < 0.05$ when compared to the DA and A fabrics at the same time point. ($n = 3$).

The inactivation data was fitted with a linear first order model to determine the rate constant of inactivation (k) for the 2 viruses (Figures S25 and S26). For both viruses, DAOH was more effective than DA in viral inactivation as demonstrated by the higher calculated k values (Table

S6, Figure 9). There were no significant differences ($p > 0.05$) between 30DAOH and 40DAOH. BVDV remained stable at RT over the 24 h duration. As such, the self-inactivation rate constant for BVDV was not reported. On the other hand, the self-inactivation rate constant for HCoV 229E averaged around 0.4 s^{-1}. k values for DAOH were around 2.3 times higher when compared to the self-inactivation rate constant of HCoV 229E.

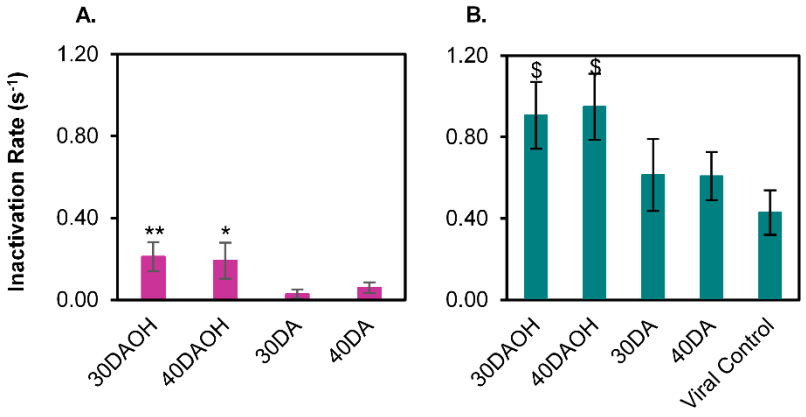

Figure 9. First order rate constants observed for (A) BVDV and (B) HCoV 229E. BVDV remained stable at RT over the 24 h duration, and the self-inactivation rate constant for BVDV was not reported. *$p < 0.05$ when compared to the 30DA. **$p < 0.05$ when compared to both DA-coated PP fabrics. $^{\$}p < 0.05$ when compared to the 40DA. ($n = 3$).

3.9. Cytotoxicity of the Polymers and Polymer-coated PP Fabrics

The cytotoxicity of the synthesized polymers and polymer-coated PP fabrics was investigated by culturing HaCaT cells directly onto these materials for 48 hours (Figure 10). The relative cell viability of DAOH and DA were around 40%, which increased to be greater than 70% after the addition of catalase. Catalase is a common enzyme found in many living organisms that are exposed to air and can catalyze H_2O_2 into water and oxygen [79]. Catalase has been found to effectively counteract the cytotoxicity induced by H_2O_2 in cell culture [80, 81]. The observed increase

in cell viability as a result of catalase addition suggests that the polymers' toxicity was primarily due to the release of H_2O_2. For A, which does not release H_2O_2, there was no statistical change between cell viability before and after the addition of catalase. Additionally, relative cell viability for cells exposed to A was around 50%. Prior reports have indicated that polyacrylamides can be cytotoxic depending on their hydrophilic/hydrophobic balance and degree of polymerization [82, 83]. To further enhance the biocompatibility of the polymer, future work will replace polyacrylamide with a backbone with enhanced cytocompatibility.

The cell viability of the PP fabric with and without polymer coating was not significantly different. In the absence of catalase, DAOH and DA coated fabrics demonstrated cell viability around 60%, which increased to above 70% after the addition of catalase. For control fabrics that do not release H_2O_2, there were no significant changes in cell viability with and without catalase. Similar to exposing cells directly to the H_2O_2-releasing polymers, catalase counteracted the cytotoxicity of H_2O_2 *in vitro*.

Although H_2O_2 generated from our polymers contributed to the observed *in vitro* cytotoxicity, the amount of generated H_2O_2 (2-4 mM) is 3 orders of magnitude lower when compared to the concentration of H_2O_2 (3w/v% or 880 mM) found in commonly used household products such as mouthwash, cerumen removal solutions, and fabric and surface disinfectants [75]. Additionally, biomaterials that generated millimolar concentrations of H_2O_2 were found to be biocompatible in subcutaneous implantation studies [38, 84]. Furthermore, H_2O_2 is generated endogenously during the wide variety of normal metabolic processes, such as mitochondrial respiration, cell signaling, and wound healing [85-87]. Cell culture media are also devoid of antioxidant enzymes that can counteract the toxicity of H_2O_2 or regulate H_2O_2 concentrations. As such, the observed cytotoxicity of H_2O_2 is not a major concern when utilizing the ROS as a disinfectant.

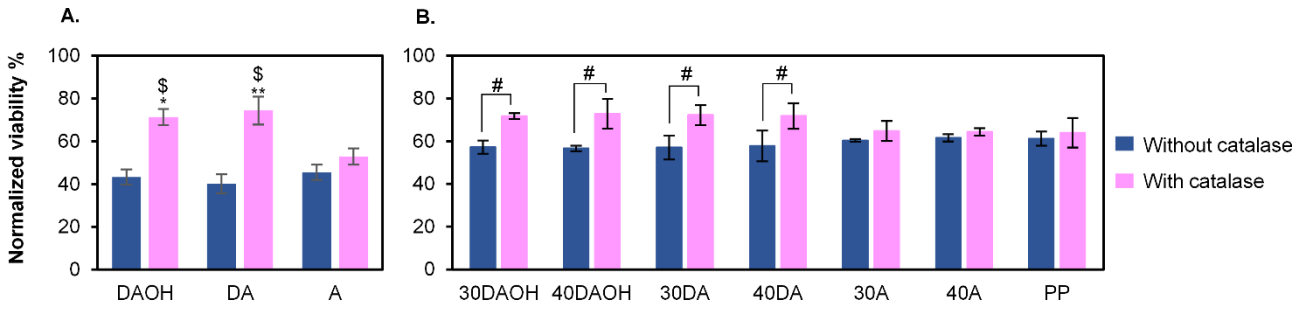

Figure 10. Normalized viability% of HaCaT cells when exposed to (A) polymers and (B) uncoated and polymer-coated PP fabrics after 48 h. *$p < 0.05$ when compared to the DAOH, **$p < 0.05$ when compared to the DA, and $^{\$}p < 0.05$ when compared to A without catalase. $^{\#}p < 0.05$ when each sample compared to its value without catalase. (n = 3).

Taken together, we developed a novel, self-disinfecting coating that could be activated by moisture added to the coating surface. Incorporation of electron donating -OH group to catechol significantly enhanced the rate of catechol autoxidation and H_2O_2 generation when compared to the unmodified catechol. In our previous work, unmodified catechol generated sufficient H_2O_2 to disinfect bacteria and viruses when the catechol-containing biomaterials were fully submerged in an aqueous solution [40-42]. However, when coated onto a surface, unmodified catechol is not effective in disinfecting these pathogens when hydrated using only a limited amount of liquid, due to its inability to generate sufficient amounts of H_2O_2. On the other hand, the faster autoxidation rate of 6-OHDA enabled DAOH coatings to rapidly generate antipathogenic levels of H_2O_2 utilizing a small water droplet. Although inactivation of bacteria and viruses was demonstrated using aqueous solutions with a volume as little as 100 µL (diameter ~ 5.76 mm for a sphere) and Video S2 demonstrated the generation of H_2O_2 using water droplets under 1,000 µm in size, future work will be required to verify the coating's ability to disinfect pathogens found in a respiratory droplet (diameter of 5 to 1,000 µm) [3, 88-93].

Nevertheless, we reported a novel, moisture-activated coating that utilizes a unique biomimetic redox chemistry. While there are numerous antipathogenic surfaces that are being developed, self-disinfecting coatings that become activated only when their antipathogenic properties are needed could be highly advantageous [18, 94, 95]. These coatings can potentially minimize users' unintended exposure to the disinfectants. However, existing self-disinfecting coatings are activated by externally applied stimuli such as heat [16] and light [17, 96], which is impractical. Our moisture-activated coating provides an alternative solution to these coatings and does not require a user to actively turn "on" or "off" the antipathogenic function.

This report focused on catechol's ability to generate H_2O_2 as a disinfectant. However, catechol is a robust adhesive molecule that can bind to a wide range of substrates through various types of interfacial interactions (hydrogen bonding, π-π and cation-π interactions, etc.), which could enhance the removal of circulating pathogens by trapping them within the filter or facemask material [97, 98]. Although we did not investigate the relative contribution of catechol adhesion to pathogen removal, the combination of multiple antipathogenic mechanisms will greatly enhance the efficacy of our coating. Finally, the reported coating does not contain a reservoir for H_2O_2 and the ROS was generated through hydration. This will greatly minimize hazards associated with storing and transporting the ROS-generating coating.

4. Conclusion

Polymer containing 6-OHDA was coated onto PP fabric and the coating generated antipathogenic levels of H_2O_2 when hydrated with a water droplet with a volume as small as 100 μL. The generated H_2O_2 successfully disinfected both Gram-positive (*S. aureus and S. epidermidis*) and Gram-negative (*P. aeruginosa and E. coli*) bacteria and model viruses, BVDV and HCoV 229E. 6-OHDA is modified with electron donating hydroxyl group, which greatly

enhanced its rate of autoxidation and H_2O_2 generation when compared to the unmodified catechol. The reported coating can potentially function as a moisture-activated, self-disinfecting coating for disinfecting pathogens on its surface.

ASSOCIATED CONTENT

Supporting Information.

Additional information regarding chemical structure of polymers, characterizations, antibacterial and antiviral activity of the PP fabric is provided (PDF).

Demonstration of coating stability test by roughly wrinkling and rubbing the polymer-coated fabric (Video S1) (MP4).

Demonstration of the rapid H_2O_2 generation by hydration of the DAOH-coated PP fabric through spraying peroxide (FOX) assay and PBS mixture (Video S2) (MP4).

AUTHOR INFORMATION

Corresponding Author

* Bruce P. Lee – Department of Biomedical Engineering, Michigan Technological University, Houghton, Michigan 49931, United States. (bplee@mtu.edu)

Author Contributions

The manuscript was written through contributions of all authors. All authors have given approval to the final version of the manuscript.

Funding Sources

This project was supported by the National Science Foundation under award numbers CMMI2119019 and DMR2001076, the National Institutes of Health under award number R15GM135875, the Office of Naval Research under the award number N00014-21-1-2877, the

Chemical Engineering Department at Michigan Tech, the James and Lorna Mack Chair in Bioengineering, and the Blue Cross Blue Shield of Michigan Foundation under award number 2023020027.

Notes

The authors declare no competing financial interest.

ACKNOWLEDGMENT

The electron microscopy research was performed at the Applied Chemical and Morphological Analysis Laboratory at Michigan Technological University. Electron Microscopy facility is supported by NSF MRI 1429232. The HCoV was received from BEI Resources, NIAID, NIH. Statistical assistance was received by the Michigan Tech Center for Applied Mathematics and Statistics (CAMS). Dr. Smitha Rao at the Michigan Technological University provided the HaCaT cells and access to the cell culture facility for the biocompatibility test. Dr. Xiaochu Ding at the Michigan Technological University provided help with the GPC analysis.

REFERENCES

(1) Giraud-Gatineau, A.; Colson, P.; Jimeno, M.-T.; Zandotti, C.; Ninove, L.; Boschi, C.; Lagier, J.-C.; La Scola, B.; Chaudet, H.; Raoult, D. Comparison of mortality associated with respiratory viral infections between December 2019 and March 2020 with that of the previous year in Southeastern France. *International Journal of Infectious Diseases* **2020**, *96*, 154-156. DOI: https://doi.org/10.1016/j.ijid.2020.05.001.

(2) Noor, R.; Maniha, S. M. A brief outline of respiratory viral disease outbreaks: 1889–till date on the public health perspectives. *VirusDisease* **2020**, *31* (4), 441-449. DOI: 10.1007/s13337-020-00628-5.

(3) Lee, B. U. Minimum Sizes of Respiratory Particles Carrying SARS-CoV-2 and the Possibility of Aerosol Generation. *International Journal of Environmental Research and Public Health* **2020**, *17* (19), 6960.

(4) Harrison, J.; Saccente-Kennedy, B.; Orton, C. M.; McCarthy, L. P.; Archer, J.; Symons, H. E.; Szczepanska, A.; Watson, N. A.; Browne, W. J.; Moseley, B. Emission rates, size distributions, and generation mechanism of oral respiratory droplets. *Aerosol Science and Technology* **2023**, *57* (3), 187-199.

(5) da Silva, P. G.; Nascimento, M. S. J.; Soares, R. R. G.; Sousa, S. I. V.; Mesquita, J. R. Airborne spread of infectious SARS-CoV-2: Moving forward using lessons from SARS-CoV and MERS-CoV. *Science of The Total Environment* **2021**, *764*, 142802. DOI: https://doi.org/10.1016/j.scitotenv.2020.142802.
(6) Andersson, J. What drives transmission of severe acute respiratory syndrome coronavirus 2? *Journal of Internal Medicine* **2021**, *290* (5), 949-951, https://doi.org/10.1111/joim.13335. DOI: https://doi.org/10.1111/joim.13335 (acccessed 2023/07/18).
(7) Gonzalez-Martin, C. Airborne Infectious Microorganisms☆. In *Encyclopedia of Microbiology (Fourth Edition)*, Schmidt, T. M. Ed.; Academic Press, 2019; pp 52-60.
(8) Leung, N. H. L. Transmissibility and transmission of respiratory viruses. *Nature Reviews Microbiology* **2021**, *19* (8), 528-545. DOI: 10.1038/s41579-021-00535-6.
(9) Wang, C. C.; Prather, K. A.; Sznitman, J.; Jimenez, J. L.; Lakdawala, S. S.; Tufekci, Z.; Marr, L. C. Airborne transmission of respiratory viruses. *Science 373* (6558), eabd9149. DOI: 10.1126/science.abd9149 (acccessed 2023/07/17).
(10) Castaño, N.; Cordts, S. C.; Kurosu Jalil, M.; Zhang, K. S.; Koppaka, S.; Bick, A. D.; Paul, R.; Tang, S. K. Y. Fomite Transmission, Physicochemical Origin of Virus–Surface Interactions, and Disinfection Strategies for Enveloped Viruses with Applications to SARS-CoV-2. *ACS Omega* **2021**, *6* (10), 6509-6527. DOI: 10.1021/acsomega.0c06335.
(11) Crawford, M. J.; Ramezani, S.; Jabbari, R.; Pathak, P.; Cho, H. J.; Kim, B. N.; Choi, H. Development of a novel self-sanitizing mask prototype to combat the spread of infectious disease and reduce unnecessary waste. *Scientific Reports* **2021**, *11* (1), 18213. DOI: 10.1038/s41598-021-97357-6.
(12) Sorci, M.; Fink, T. D.; Sharma, V.; Singh, S.; Chen, R.; Arduini, B. L.; Dovidenko, K.; Heldt, C. L.; Palermo, E. F.; Zha, R. H. Virucidal N95 Respirator Face Masks via Ultrathin Surface-Grafted Quaternary Ammonium Polymer Coatings. *ACS Applied Materials & Interfaces* **2022**, *14* (22), 25135-25146. DOI: 10.1021/acsami.2c04165.
(13) Weber, D. J.; Rutala, W. A. Self-disinfecting surfaces: Review of current methodologies and future prospects. *American Journal of Infection Control* **2013**, *41* (5, Supplement), S31-S35. DOI: https://doi.org/10.1016/j.ajic.2012.12.005.
(14) Mahmood, A.; Eqan, M.; Pervez, S.; Alghamdi, H. A.; Tabinda, A. B.; Yasar, A.; Brindhadevi, K.; Pugazhendhi, A. COVID-19 and frequent use of hand sanitizers; human health and environmental hazards by exposure pathways. *Science of The Total Environment* **2020**, *742*, 140561. DOI: https://doi.org/10.1016/j.scitotenv.2020.140561.
(15) Siller, P.; Reissner, J.; Hansen, S.; Kühl, M.; Bartel, A.; Schmelzeisen, D.; Gries, T.; Roesler, U.; Friese, A. Innovative Textiles Used in Face Masks: Filtration Efficiency and Self-Disinfecting Properties against Coronaviruses. In *Nanomaterials*, 2021; Vol. 11.
(16) Kumar, S.; Karmacharya, M.; Joshi, S. R.; Gulenko, O.; Park, J.; Kim, G.-H.; Cho, Y.-K. Photoactive Antiviral Face Mask with Self-Sterilization and Reusability. *Nano Letters* **2021**, *21* (1), 337-343. DOI: 10.1021/acs.nanolett.0c03725.
(17) Tang, P.; Zhang, Z.; El-Moghazy, A. Y.; Wisuthiphaet, N.; Nitin, N.; Sun, G. Daylight-Induced Antibacterial and Antiviral Cotton Cloth for Offensive Personal Protection. *ACS Applied Materials & Interfaces* **2020**, *12* (44), 49442-49451. DOI: 10.1021/acsami.0c15540.
(18) Lishchynskyi, O.; Shymborska, Y.; Stetsyshyn, Y.; Raczkowska, J.; Skirtach, A. G.; Peretiatko, T.; Budkowski, A. Passive antifouling and active self-disinfecting antiviral surfaces. *Chemical Engineering Journal* **2022**, *446*, 137048. DOI: https://doi.org/10.1016/j.cej.2022.137048.

(19) Punjabi, K.; Bhatia, E.; Keshari, R.; Jadhav, K.; Singh, S.; Shastri, J.; Banerjee, R. Biopolymer Coating Imparts Sustainable Self-Disinfecting and Antimicrobial Properties to Fabric: Translated to Protective Gears for the Pandemic and Beyond. *ACS Biomaterials Science & Engineering* **2023**, *9* (2), 1116-1131. DOI: 10.1021/acsbiomaterials.2c01481.
(20) Versoza, M.; Heo, J.; Ko, S.; Kim, M.; Park, D. Solid Oxygen-Purifying (SOP) Filters: A Self-Disinfecting Filters to Inactivate Aerosolized Viruses. In *International Journal of Environmental Research and Public Health*, 2020; Vol. 17.
(21) Tian, H.; He, B.; Yin, Y.; Liu, L.; Shi, J.; Hu, L.; Jiang, G. Chemical Nature of Metals and Metal-Based Materials in Inactivation of Viruses. *Nanomaterials* **2022**, *12* (14), 2345.
(22) Wang, L.-S.; Xu, S.; Gopal, S.; Kim, E.; Kim, D.; Brier, M.; Solanki, K.; Dordick, J. S. Facile fabrication of antibacterial and antiviral perhydrolase-polydopamine composite coatings. *Scientific Reports* **2021**, *11* (1), 12410. DOI: 10.1038/s41598-021-91925-6.
(23) Querido, M. M.; Aguiar, L.; Neves, P.; Pereira, C. C.; Teixeira, J. P. Self-disinfecting surfaces and infection control. *Colloids and Surfaces B: Biointerfaces* **2019**, *178*, 8-21. DOI: https://doi.org/10.1016/j.colsurfb.2019.02.009.
(24) Siller, P.; Reissner, J.; Hansen, S.; Kühl, M.; Bartel, A.; Schmelzeisen, D.; Gries, T.; Roesler, U.; Friese, A. Innovative Textiles Used in Face Masks: Filtration Efficiency and Self-Disinfecting Properties against Coronaviruses. *Nanomaterials* **2021**, *11* (8), 2088.
(25) Li, H.; Li, N.; Yang, Y.; Zhang, L.; Bai, W.; Zhang, X.; Xu, Y.; Li, Y. Self-sterilization and self-powered real-time respiratory monitoring of reusable masks engineered by bioinspired coatings. *Nano Energy* **2023**, *115*, 108750. DOI: https://doi.org/10.1016/j.nanoen.2023.108750.
(26) Winterbourn, C. C. Reconciling the chemistry and biology of reactive oxygen species. *Nature Chemical Biology* **2008**, *4* (5), 278-286. DOI: 10.1038/nchembio.85.
(27) Sheriff, T. S. Applications of hydrogen peroxide and derivatives. By C W Jones, RSC Clean Technology Monographs, Series Editor James H Clark, Royal Society of Chemistry, pp viii + 264 ISBN 085404536-8. *Journal of Chemical Technology & Biotechnology* **2000**, *75* (11), 1083-1083, https://doi.org/10.1002/1097-4660(200011)75:11<1083::AID-JCTB295>3.0.CO;2-G. DOI: https://doi.org/10.1002/1097-4660(200011)75:11<1083::AID-JCTB295>3.0.CO;2-G (acccessed 2022/07/17).
(28) Alt, E.; Leipold, F.; Milatovic, D.; Lehmann, G.; Heinz, S.; Schömig, A. Hydrogen peroxide for prevention of bacterial growth on polymer biomaterials. *Ann Thorac Surg* **1999**, *68* (6), 2123-2128. DOI: 10.1016/s0003-4975(99)00832-2 From NLM.
(29) Repine, J. E.; Fox, R. B.; Berger, E. M. Hydrogen peroxide kills Staphylococcus aureus by reacting with staphylococcal iron to form hydroxyl radical. *J Biol Chem* **1981**, *256* (14), 7094-7096. From NLM.
(30) McDonnell, G. The Use of Hydrogen Peroxide for Disinfection and Sterilization Applications. In *Patai's Chemistry of Functional Groups*, pp 1-34.
(31) Kord Forooshani, P.; Lee, B. P. Recent approaches in designing bioadhesive materials inspired by mussel adhesive protein. *Journal of Polymer Science Part A: Polymer Chemistry* **2017**, *55* (1), 9-33. DOI: https://doi.org/10.1002/pola.28368.
(32) Lee, B. P.; Messersmith, P. B.; Israelachvili, J. N.; Waite, J. H. Mussel-Inspired Adhesives and Coatings. *Annu Rev Mater Res* **2011**, *41*, 99-132. DOI: 10.1146/annurev-matsci-062910-100429 From NLM.
(33) Li, L.; Zeng, H. Marine mussel adhesion and bio-inspired wet adhesives. *Biotribology* **2016**, *5*, 44-51. DOI: https://doi.org/10.1016/j.biotri.2015.09.004.

(34) Sedó, J.; Saiz-Poseu, J.; Busqué, F.; Ruiz-Molina, D. Catechol-Based Biomimetic Functional Materials. *Adv. Mat.* **2013**, *25* (5), 653-701. DOI: 10.1002/adma.201202343.
(35) Kaushik, N. K.; Kaushik, N.; Pardeshi, S.; Sharma, J. G.; Lee, S. H.; Choi, E. H. Biomedical and Clinical Importance of Mussel-Inspired Polymers and Materials. *Marine Drugs* **2015**, *13* (11), 6792-6817.
(36) Pinnataip, R.; Lee, B. P. Oxidation Chemistry of Catechol Utilized in Designing Stimuli-Responsive Adhesives and Antipathogenic Biomaterials. *ACS Omega* **2021**, *6* (8), 5113-5118. DOI: 10.1021/acsomega.1c00006.
(37) Razaviamri, S.; Wang, K.; Liu, B.; Lee, B. P. Catechol-Based Antimicrobial Polymers. In *Molecules*, 2021; Vol. 26.
(38) Meng, H.; Li, Y.; Faust, M.; Konst, S.; Lee, B. P. Hydrogen peroxide generation and biocompatibility of hydrogel-bound mussel adhesive moiety. *Acta Biomater.* **2015**, *17*, 160-169.
(39) Meng, H.; Liu, Y.; Lee, B. P. Model polymer system for investigating the generation of hydrogen peroxide and its biological responses during the crosslinking of mussel adhesive moiety. *Acta Biomaterialia* **2017**, *48*, 144-156. DOI: https://doi.org/10.1016/j.actbio.2016.10.016.
(40) Meng, H.; Forooshani, P. K.; Joshi, P. U.; Osborne, J.; Mi, X.; Meingast, C.; Pinnaratip, R.; Kelley, J.; Narkar, A.; He, W.; et al. Biomimetic recyclable microgels for on-demand generation of hydrogen peroxide and antipathogenic application. *Acta Biomaterialia* **2019**, *83*, 109-118. DOI: https://doi.org/10.1016/j.actbio.2018.10.037.
(41) Kord Forooshani, P.; Polega, E.; Thomson, K.; Bhuiyan, M. S. A.; Pinnaratip, R.; Trought, M.; Kendrick, C.; Gao, Y.; Perrine, K. A.; Pan, L.; et al. Antibacterial Properties of Mussel-Inspired Polydopamine Coatings Prepared by a Simple Two-Step Shaking-Assisted Method. *Frontiers in Chemistry* **2019**, *7*, Original Research. DOI: 10.3389/fchem.2019.00631.
(42) Kord Forooshani, P.; Pinnaratip, R.; Polega, E.; Tyo, A. G.; Pearson, E.; Liu, B.; Folayan, T.-O.; Pan, L.; Rajachar, R. M.; Heldt, C. L.; et al. Hydroxyl Radical Generation through the Fenton-like Reaction of Hematin- and Catechol-Functionalized Microgels. *Chemistry of Materials* **2020**, *32* (19), 8182-8194. DOI: 10.1021/acs.chemmater.0c01551.
(43) Zhang, Z.; He, X.; Zhou, C.; Reaume, M.; Wu, M.; Liu, B.; Lee, B. P. Iron Magnetic Nanoparticle-Induced ROS Generation from Catechol-Containing Microgel for Environmental and Biomedical Applications. *ACS Appl. Mater. Interfaces* **2020**, *12* (19), 21210-21220. DOI: 10.1021/acsami.9b19726.
(44) Menyo, M. S.; Hawker, C. J.; Waite, J. H. Versatile tuning of supramolecular hydrogels through metal complexation of oxidation-resistant catechol-inspired ligands. *Soft Matter* **2013**, *9* (43), 10314-10323, 10.1039/C3SM51824H. DOI: 10.1039/C3SM51824H.
(45) Amstad, E.; Gehring, A. U.; Fischer, H.; Nagaiyanallur, V. V.; Hähner, G.; Textor, M.; Reimhult, E. Influence of Electronegative Substituents on the Binding Affinity of Catechol-Derived Anchors to Fe3O4 Nanoparticles. *The Journal of Physical Chemistry C* **2011**, *115* (3), 683-691. DOI: 10.1021/jp1109306.
(46) Liu, B.; Zhou, C.; Zhang, Z.; Roland, J. D.; Lee, B. P. Antimicrobial property of halogenated catechols. *Chemical Engineering Journal* **2021**, *403*, 126340. DOI: https://doi.org/10.1016/j.cej.2020.126340.
(47) Amstad, E.; Gillich, T.; Bilecka, I.; Textor, M.; Reimhult, E. Ultrastable Iron Oxide Nanoparticle Colloidal Suspensions Using Dispersants with Catechol-Derived Anchor Groups. *Nano Letters* **2009**, *9* (12), 4042-4048. DOI: 10.1021/nl902212q.

(48) Liang, Y. O.; Wightman, R. M.; Adams, R. N. Competitive oxidation of 6-hydroxydopamine by oxygen and hydrogen peroxide. *European Journal of Pharmacology* **1976**, *36* (2), 455-458. DOI: https://doi.org/10.1016/0014-2999(76)90102-3.
(49) Padiglia, A.; Medda, R.; Lorrai, A.; Biggio, G.; Sanna, E.; Floris, G. Modulation of 6-hydroxydopamine oxidation by various proteins. *Biochem. Pharmacol.* **1997**, *53* (8), 1065-1068. DOI: https://doi.org/10.1016/S0006-2952(96)00716-2.
(50) Lee, H.; Lee, B. P.; Messersmith, P. B. A reversible wet/dry adhesive inspired by mussels and geckos. *Nature* **2007**, *448* (7151), 338-341. DOI: 10.1038/nature05968.
(51) Raghavan, P.; Zhao, X.; Kim, J.-K.; Manuel, J.; Chauhan, G. S.; Ahn, J.-H.; Nah, C. Ionic conductivity and electrochemical properties of nanocomposite polymer electrolytes based on electrospun poly(vinylidene fluoride-co-hexafluoropropylene) with nano-sized ceramic fillers. *Electrochimica Acta* **2008**, *54* (2), 228-234. DOI: https://doi.org/10.1016/j.electacta.2008.08.007.
(52) Häntzschel, N.; Hund, R.-D.; Hund, H.; Schrinner, M.; Lück, C.; Pich, A. Hybrid Microgels with Antibacterial Properties. *Macromolecular Bioscience* **2009**, *9* (5), 444-449, https://doi.org/10.1002/mabi.200800219. DOI: https://doi.org/10.1002/mabi.200800219 (acccessed 2023/07/17).
(53) Vilčnik, A.; Jerman, I.; Šurca Vuk, A.; Koželj, M.; Orel, B.; Tomšič, B.; Simončič, B.; Kovač, J. Structural Properties and Antibacterial Effects of Hydrophobic and Oleophobic Sol−Gel Coatings for Cotton Fabrics. *Langmuir* **2009**, *25* (10), 5869-5880. DOI: 10.1021/la803742c.
(54) Heldt, C. L.; Hernandez, R.; Mudiganti, U.; Gurgel, P. V.; Brown, D. T.; Carbonell, R. G. A colorimetric assay for viral agents that produce cytopathic effects. *Journal of Virological Methods* **2006**, *135* (1), 56-65. DOI: https://doi.org/10.1016/j.jviromet.2006.01.022.
(55) Tafur, M. F.; Vijayaragavan, K. S.; Heldt, C. L. Reduction of porcine parvovirus infectivity in the presence of protecting osmolytes. *Antiviral Research* **2013**, *99* (1), 27-33. DOI: https://doi.org/10.1016/j.antiviral.2013.04.019.
(56) Chen, J. L.; Steele, T. W. J.; Stuckey, D. C. Metabolic reduction of resazurin; location within the cell for cytotoxicity assays. *Biotechnology and Bioengineering* **2018**, *115* (2), 351-358. DOI: https://doi.org/10.1002/bit.26475.
(57) Lee, B. P.; Huang, K.; Nunalee, F. N.; Shull, K. R.; Messersmith, P. B. Synthesis of 3,4-Dihydroxyphenylalanine (DOPA) Containing Monomers and Their Copolymerization with PEG-Diacrylate to from Hydrogels. *J. Biomater. Sci., Polym. Ed.* **2004**, *15*, 449-464.
(58) Lee, B. P.; Chao, C.-Y.; Nunalee, F. N.; Motan, E.; Shull, K. R.; Messersmith, P. B. Rapid Gel Formation and Adhesion in Photocurable and Biodegradable Block Copolymers with High DOPA Content. *Macromol.* **2006**, *39* (5), 1740-1748. DOI: 10.1021/ma0518959 (acccessed 2013/12/08).
(59) Du, W.; Iacoviello, F.; Fernandez, T.; Loureiro, R.; Brett, D. J. L.; Shearing, P. R. Microstructure analysis and image-based modelling of face masks for COVID-19 virus protection. *Communications Materials* **2021**, *2* (1), 69. DOI: 10.1038/s43246-021-00160-z.
(60) Bhardwaj, R.; Agrawal, A. Tailoring surface wettability to reduce chances of infection of COVID-19 by a respiratory droplet and to improve the effectiveness of personal protection equipment. *Physics of Fluids* **2020**, *32* (8). DOI: 10.1063/5.0020249 (acccessed 11/13/2023).
(61) Melayil, K. R.; Mitra, S. K. Wetting, Adhesion, and Droplet Impact on Face Masks. *Langmuir* **2021**, *37* (8), 2810-2815. DOI: 10.1021/acs.langmuir.0c03556.

(62) Cigana, C.; Bianconi, I.; Baldan, R.; De Simone, M.; Riva, C.; Sipione, B.; Rossi, G.; Cirillo, D. M.; Bragonzi, A. Staphylococcus aureus Impacts Pseudomonas aeruginosa Chronic Respiratory Disease in Murine Models. *The Journal of Infectious Diseases* **2017**, *217* (6), 933-942. DOI: 10.1093/infdis/jix621 (acccessed 11/26/2023).
(63) Ortega-Peña, S.; Rodríguez-Martínez, S.; Cancino-Diaz, M. E.; Cancino-Diaz, J. C. Staphylococcus epidermidis Controls Opportunistic Pathogens in the Nose, Could It Help to Regulate SARS-CoV-2 (COVID-19) Infection? *Life* **2022**, *12* (3), 341.
(64) Edwards, B. D.; Somayaji, R.; Greysson-Wong, J.; Izydorczyk, C.; Waddell, B.; Storey, D. G.; Rabin, H. R.; Surette, M. G.; Parkins, M. D. Clinical Outcomes Associated With Escherichia coli Infections in Adults With Cystic Fibrosis: A Cohort Study. *Open Forum Infectious Diseases* **2019**, *7* (1). DOI: 10.1093/ofid/ofz476 (acccessed 11/26/2023).
(65) Xie, Z.; Peng, Y.; Li, C.; Luo, X.; Wei, Z.; Li, X.; Yao, Y.; Fang, T.; Huang, L. Growth kinetics of Staphylococcus aureus and background microorganisms in camel milk. *Journal of Dairy Science* **2020**, *103* (11), 9958-9968. DOI: https://doi.org/10.3168/jds.2020-18616.
(66) Bronikowski, A. M.; Bennett, A. F.; Lenski, R. E. EVOLUTIONARY ADAPTATION TO TEMPERATURE. VIII. EFFECTS OF TEMPERATURE ON GROWTH RATE IN NATURAL ISOLATES OF ESCHERICHIA COLI AND SALMONELLA ENTERICA FROM DIFFERENT THERMAL ENVIRONMENTS. *Evolution* **2001**, *55* (1), 33-40. DOI: https://doi.org/10.1111/j.0014-3820.2001.tb01270.x.
(67) LaBauve, A. E.; Wargo, M. J. Growth and laboratory maintenance of Pseudomonas aeruginosa. *Curr Protoc Microbiol* **2012**, *Chapter 6*, Unit 6E.1. DOI: 10.1002/9780471729259.mc06e01s25 From NLM.
(68) Fournière, M.; Latire, T.; Souak, D.; Feuilloley, M. G. J.; Bedoux, G. Staphylococcus epidermidis and Cutibacterium acnes: Two Major Sentinels of Skin Microbiota and the Influence of Cosmetics. *Microorganisms* **2020**, *8* (11). DOI: 10.3390/microorganisms8111752 From NLM.
(69) Alt, E.; Leipold, F.; Milatovic, D.; Lehmann, G.; Heinz, S.; Schömig, A. Hydrogen peroxide for prevention of bacterial growth on polymer biomaterials. *The Annals of Thoracic Surgery* **1999**, *68* (6), 2123-2128. DOI: https://doi.org/10.1016/S0003-4975(99)00832-2.
(70) Zhu, Y.; Xu, H.; Yang, X.; Zhuang, J.; Wang, Y.; Feng, J.; Ma, R.; Jiao, Z. The synergistic antibacterial activity and mechanism of ultrasound and hydrogen peroxide against Staphylococcus aureus in water. *Journal of Water Process Engineering* **2022**, *50*, 103349. DOI: https://doi.org/10.1016/j.jwpe.2022.103349.
(71) Han, B.; Han, X.; Ren, M.; You, Y.; Zhan, J.; Huang, W. Antimicrobial Effects of Novel H2O2-Ag+ Complex on Membrane Damage to Staphylococcus aureus, Escherichia coli O157:H7, and Salmonella Typhimurium. *Journal of Food Protection* **2022**, *85* (1), 104-111. DOI: https://doi.org/10.4315/JFP-21-087.
(72) Henderson, E.; Schneider, S.; Petersen, F. C.; Haugen, H. J.; Wohlfahrt, J. C.; Ekstrand, K.; Ekfeldt, A. Chemical debridement of contaminated titanium surfaces: An in vitro study. *Acta Odontologica Scandinavica* **2013**, *71* (3-4), 957-964. DOI: 10.3109/00016357.2012.734423.
(73) Huang, T.; Sui, M.; Li, J. Inactivation of E. coli by nano-Cu/MWCNTs combined with hydrogen peroxide. *Science of The Total Environment* **2017**, *574*, 818-828. DOI: https://doi.org/10.1016/j.scitotenv.2016.09.077.

(74) Sultana, S. T.; Call, D. R.; Beyenal, H. Eradication of Pseudomonas aeruginosa biofilms and persister cells using an electrochemical scaffold and enhanced antibiotic susceptibility. *npj Biofilms and Microbiomes* **2016**, *2* (1), 2. DOI: 10.1038/s41522-016-0003-0.
(75) Watt, B. E.; Proudfoot, A. T.; Vale, J. A. Hydrogen Peroxide Poisoning. *Toxicological Reviews* **2004**, *23* (1), 51-57. DOI: 10.2165/00139709-200423010-00006.
(76) Mulabbi, E. N.; Tweyongyere, R.; Byarugaba, D. K. The history of the emergence and transmission of human coronaviruses. *Onderstepoort J Vet Res* **2021**, *88* (1), e1-e8. DOI: 10.4102/ojvr.v88i1.1872 From NLM.
(77) Wang, X.; Tarabara, V. V. Virus adhesion to archetypal fomites: A study with human adenovirus and human respiratory syncytial virus. *Chemical Engineering Journal* **2022**, *429*, 132085. DOI: https://doi.org/10.1016/j.cej.2021.132085.
(78) Tsutsumi-Arai, C.; Iwamiya, Y.; Hoshino, R.; Terada-Ito, C.; Sejima, S.; Akutsu-Suyama, K.; Shibayama, M.; Hiroi, Z.; Tokuyama-Toda, R.; Iwamiya, R.; et al. Surface Functionalization of Non-Woven Fabrics Using a Novel Silica-Resin Coating Technology: Antiviral Treatment of Non-Woven Fabric Filters in Surgical Masks. In *International Journal of Environmental Research and Public Health*, 2022; Vol. 19.
(79) Chelikani, P.; Fita, I.; Loewen, P. C. Diversity of structures and properties among catalases. *CMLS, Cell. Mol. Life Sci.* **2004**, *61* (2), 192-208. DOI: 10.1007/s00018-003-3206-5.
(80) Chai, P. C.; Long, L. H.; Halliwell, B. Contribution of hydrogen peroxide to the cytotoxicity of green tea and red wines. *Biochemical and Biophysical Research Communications* **2003**, *304* (4), 650-654. DOI: http://dx.doi.org/10.1016/S0006-291X(03)00655-7.
(81) Clement, M.-V.; Long, L. H.; Ramalingam, J.; Halliwell, B. The cytotoxicity of dopamine may be an artefact of cell culture. *Journal of Neurochemistry* **2002**, *81* (3), 414-421. DOI: 10.1046/j.1471-4159.2002.00802.x.
(82) Schaefer, S.; Pham, T. T. P.; Brunke, S.; Hube, B.; Jung, K.; Lenardon, M. D.; Boyer, C. Rational Design of an Antifungal Polyacrylamide Library with Reduced Host-Cell Toxicity. *ACS Applied Materials & Interfaces* **2021**, *13* (23), 27430-27444. DOI: 10.1021/acsami.1c05020.
(83) Nowak, A.; Zakłos-Szyda, M.; Żyżelewicz, D.; Koszucka, A.; Motyl, I. Acrylamide Decreases Cell Viability, and Provides Oxidative Stress, DNA Damage, and Apoptosis in Human Colon Adenocarcinoma Cell Line Caco-2. *Molecules* **2020**, *25* (2), 368.
(84) Meng, H.; Liu, Y.; Lee, B. P. Model polymer system for investigating the generation of hydrogen peroxide and its biological responses during the crosslinking of mussel adhesive moiety. *Acta Biomater.* **2017**, *48*, 144-156. DOI: http://dx.doi.org/10.1016/j.actbio.2016.10.016.
(85) Bryan, N.; Ahswin, H.; Smart, N.; Bayon, Y.; Wohlert, S.; Hunt, J. A. Reactive oxygen species (ROS)–a family of fate deciding molecules pivotal in constructive inflammation and wound healing. *Eur. Cells Mater.* **2012**, *24* (249), e65.
(86) Pullar, J. M.; Vissers, M.; Winterbourn, C. C. Living with a killer: the effects of hypochlorous acid on mammalian cells. *IUBMB life* **2000**, *50* (4-5), 259-266.
(87) Anderson, J. M. Biological Responses to Materials. *Annu. Rev. Mater. Res.* **2001**, *31* (1), 81-110. DOI: 10.1146/annurev.matsci.31.1.81.
(88) Duguid, J. P. The size and the duration of air-carriage of respiratory droplets and droplet-nuclei. *Journal of Hygiene* **1946**, *44* (6), 471-479. DOI: 10.1017/S0022172400019288 From Cambridge University Press Cambridge Core.

(89) Holmgren, H.; Ljungström, E.; Almstrand, A.-C.; Bake, B.; Olin, A.-C. Size distribution of exhaled particles in the range from 0.01 to 2.0μm. *Journal of Aerosol Science* **2010**, *41* (5), 439-446. DOI: https://doi.org/10.1016/j.jaerosci.2010.02.011.
(90) Papineni, R. S.; Rosenthal, F. S. The Size Distribution of Droplets in the Exhaled Breath of Healthy Human Subjects. *Journal of Aerosol Medicine* **1997**, *10* (2), 105-116. DOI: 10.1089/jam.1997.10.105.
(91) Loudon, R. G.; Roberts, R. M. Relation between the Airborne Diameters of Respiratory Droplets and the Diameter of the Stains left after Recovery. *Nature* **1967**, *213* (5071), 95-96. DOI: 10.1038/213095a0.
(92) Stilianakis, N. I.; Drossinos, Y. Dynamics of infectious disease transmission by inhalable respiratory droplets. *Journal of The Royal Society Interface* **2010**, *7* (50), 1355-1366. DOI: doi:10.1098/rsif.2010.0026.
(93) Duguid, J. P. The size and the duration of air-carriage of respiratory droplets and droplet-nuclei. *Epidemiology and Infection* **1946**, *44* (6), 471-479. DOI: 10.1017/S0022172400019288 From Cambridge University Press Cambridge Core.
(94) Dahanayake, M. H.; Athukorala, S. S.; Jayasundera, A. C. A. Recent breakthroughs in nanostructured antiviral coating and filtration materials: a brief review. *RSC Advances* **2022**, *12* (26), 16369-16385, 10.1039/D2RA01567F. DOI: 10.1039/D2RA01567F.
(95) Bregnocchi, A.; Jafari, R.; Momen, G. Design strategies for antiviral coatings and surfaces: A review. *Applied Surface Science Advances* **2022**, *8*, 100224. DOI: https://doi.org/10.1016/j.apsadv.2022.100224.
(96) Sunada, K.; Minoshima, M.; Hashimoto, K. Highly efficient antiviral and antibacterial activities of solid-state cuprous compounds. *Journal of Hazardous Materials* **2012**, *235-236*, 265-270. DOI: https://doi.org/10.1016/j.jhazmat.2012.07.052.
(97) Kim, S.; Chung, J.; Lee, S. H.; Yoon, J. H.; Kweon, D.-H.; Chung, W.-J. Tannic acid-functionalized HEPA filter materials for influenza virus capture. *Scientific Reports* **2021**, *11* (1), 979. DOI: 10.1038/s41598-020-78929-4.
(98) White, E. HEPA and ULPA filters. *Journal of Validation Technology* **2009**, *15* (3), 48.

TOC

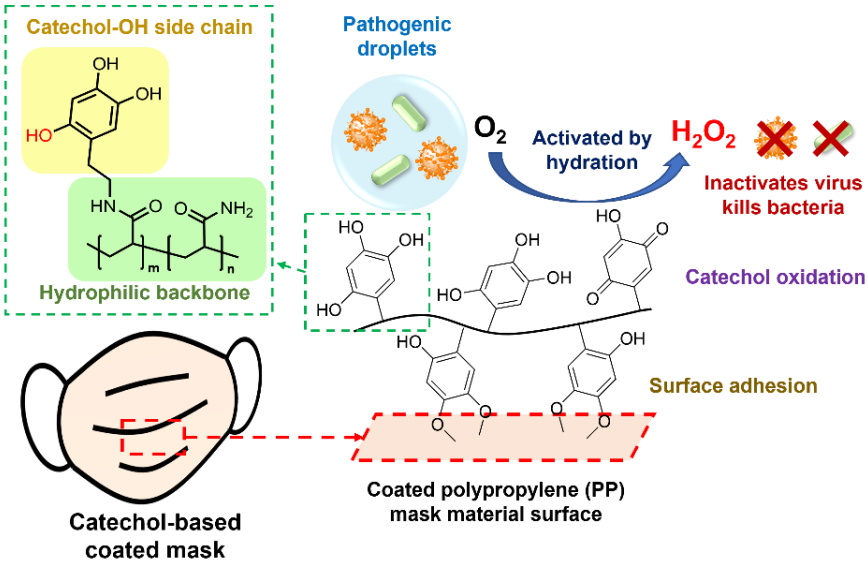
Catechol-OH side chain
Hydrophilic backbone
Pathogenic droplets
O_2
Activated by hydration
H_2O_2
Inactivates virus kills bacteria
Catechol oxidation
Surface adhesion
Coated polypropylene (PP) mask material surface
Catechol-based coated mask